Gene profile of zebrafish fin regeneration offers clues to kinetics, organization and biomechanics of basement membrane

Pauline Nauroy, Alexandre Guiraud, Julien Chlasta, Marilyne Malbouyres, Benjamin Gillet, Sandrine Hughes, Elise Lambert, Florence Ruggiero

GENE PROFILE OF ZEBRAFISH FIN REGENERATION OFFERS CLUES TO KINETICS, ORGANIZATION AND BIOMECHANICS OF BASEMENT MEMBRANE

Pauline Nauroy[1], Alexandre Guiraud[1], Julien Chlasta[2], Marilyne Malbouyres[1], Benjamin Gillet[1], Sandrine Hughes[1], Elise Lambert[1], and Florence Ruggiero[1*]

[1] Université de Lyon, ENSL, CNRS, Institut de Génomique Fonctionnelle de Lyon, 46 allée d'Italie F-69364 Lyon, France.

[2] BioMeca, ENSL, Université de Lyon, 46 allée d'Italie F-69364 Lyon, France.

[*] corresponding authors
Florence Ruggiero

Institut de Génomique Fonctionnelle de Lyon - ENS de Lyon

46 Allée d'Italie

F69364 Lyon cedex 07

France

Phone number: +33 472722657

Fax number: +33 472722602

e-mail: florence.ruggiero@ens-lyon.fr

Abstract

How some animals regenerate missing body parts is not well understood. Taking advantage of the zebrafish caudal fin model, we performed a global unbiased time-course transcriptomic analysis of fin regeneration. Biostatistics analyses identified extracellular matrix (ECM) as the most enriched gene sets. Basement membranes (BMs) are specialized ECM structures that provide tissues with structural cohesion and serve as a major extracellular signaling platform. While the embryonic formation of BM has been extensively investigated, its regeneration in adults remains poorly studied. We therefore focused on BM gene expression kinetics and showed that it recapitulates many aspects of development. As such, the re-expression of the embryonic *col14a1a* gene indicated that *col14a1a* is part of the regeneration-specific program. We showed that laminins and *col14a1a* genes display similar kinetics and that the corresponding proteins are spatially and temporally controlled during regeneration. Analysis of our CRISPR/Cas9-mediated *col14a1a* knockout fish showed that collagen XIV-A contributes to timely deposition of laminins. As changes in ECM organization can affect tissue mechanical properties, we analyzed the biomechanics of *col14a1a*$^{-/-}$ regenerative BM using atomic force microscopy (AFM). Our data revealed a thinner BM accompanied by a substantial increase of the stiffness when compared to controls. Further AFM 3D-reconstructions showed that BM is organized as a checkerboard made of alternation of soft and rigid regions that is compromised in mutants leading to a more compact structure. We conclude that collagen XIV-A transiently acts as a molecular spacer responsible for BM structure and biomechanics possibly by helping laminins integration within regenerative BM.

Keywords

extracellular matrix, collagen XIV, basement membrane, zebrafish, regeneration, transcriptome

Abbreviations

ECM, Extracellular Matrix; BM, Basement Membrane; BMZ, Basement Membrane Zone; dpa, days post amputation; FACIT, Fibrillar Associated Collagen with Interrupted Triple Helix; ColXIV-A, collagen XIV-A; ColXII, Collagen XII; MO, Morpholinos; AFM, atomic force microscopy; PCA, Principal Component Analysis; GO, Gene Ontology; TEM, transmission electron microscopy.

1. Introduction

The zebrafish is one of the main regeneration-competent vertebrates and, as such, became in the last decade, an instrumental model for understanding regeneration mechanisms. Adult zebrafish are able to regenerate several organs including heart, spinal cord, retina, brain and appendages. Due to its simple structure, accessibility and fast regeneration, caudal fin has become one of the most popular model for regeneration [1,2]. After fin amputation, epidermal cells migrate from the stump margins and forms a wound epidermis that covers the exposed stump and results in the blastema formation. Fin then grows and tissues differentiate in a proximo-distal way until complete fin regeneration [2,3]. We thus took advantage of the zebrafish caudal fin regeneration model to perform a global unbiased time-course transcriptomic analysis in order to investigate the genes involved in this process. Bioinformatics analyses of the RNA-seq revealed that among the large number of genes differentially expressed during regeneration, the most enriched gene sets are related to extracellular matrix (ECM) structure and organization.

Extracellular matrix makes up cells microenvironment and plays key instructive role in controlling and integrating diverse cellular functions. ECM components are integral to embryonic development and several physiological and pathological processes. Basement membranes (BMs) are specialized ECM structures that provide tissues with structural cohesion and serve as a major extracellular signaling platform. BMs are found in the most primitive multicellular organisms [4] and they are essential for a large number of biological processes including development, tissue homeostasis and tissue repair [5,6]. The structure and organization of BM are well characterized, and the components essential to BM network formation, *i.e.* collagen IV, laminins, perlecan and nidogens, were referred to as the BM toolkit [7]. In epidermis, BM separates epithelia from the underlying dermal connective tissue and extends to a region called basement membrane zone (BMZ) that includes ECM proteins of the epidermal-dermal junction that are not part of the BM toolkit. The functional contribution of each of the components of the BMZ is far to be elucidated. While the formation, development and repair of BM have been extensively investigated [8], BM regeneration in adults remains poorly studied [9]. In particular the question of whether BM regeneration recapitulates BM development has not been addressed yet.

Analyses of the RNA-seq results using the proteomic definition of the BM by Randles and collaborators [10] and the *in-silico* zebrafish matrisome we recently defined [11] revealed that BM

regeneration recapitulates many aspects of its development including re-expression of embryonic genes. As such, *col14a1a* that we previously characterized as an embryonic epidermal BMZ component [12], was sharply expressed from 2 days post amputation (dpa) allowing further analysis of the role of its protein product, collagen XIV-A (ColXIV-A), in regeneration. In mice, Collagen XIV, a member of the Fibrillar Associated Collagen with Interrupted Triple Helix (FACIT) subset of the collagen superfamily is required for tendon fibrillogenesis, cornea endothelial maturation and myocardium integrity [13–15]. Collagen XIV was also found associated with the human epidermal BM during skin development [16] and, more recently, the zebrafish paralogue *col14a1a* was shown to be transiently expressed in the BMZ at early stages of zebrafish development [12]. Morpholinos (MO) knockdown of ColXIV-A in zebrafish embryos led to defects in embryonic BM structure [12]. To deeper study the role of this gene in regeneration, we generated a CRISPR/Cas9 *col14a1a*$^{-/-}$ line in which *col14a1a* expression is abolished. While *col14a1a* expression did not seem to be critically required for development, the initiation of BM formation or global integrity of the outgrowth, ColXIV-A appeared to be a regulator of BM structural organization and biomechanics. Based on atomic force microscopy (AFM) tomography experiments, we proposed that ColXIV-A acts as a molecular spacer that is transiently but specifically required for the proper three-dimensional organization of regenerative BM.

2. Results

2.1. Transcriptional profiling of zebrafish caudal fin regeneration reveals signatures of ECM remodeling

To investigate gene expression profile during regeneration, we performed a global unbiased time-course transcriptomic analysis using RNA-seq. Total RNA was extracted from regenerating caudal fins at various time points: 0 dpa corresponding to the uncut adult fin; 2 dpa and 3 dpa, when the regeneration program is installed and regenerative outgrowth continues growing; and finally at 10 dpa which corresponds to a late phase of regeneration (Figure 1a and Figure S1). Principal Component Analysis (PCA) of RNA-seq data showed that the biological replicates tightly cluster, validating the coherence of the experimental procedure (Figure 1b).

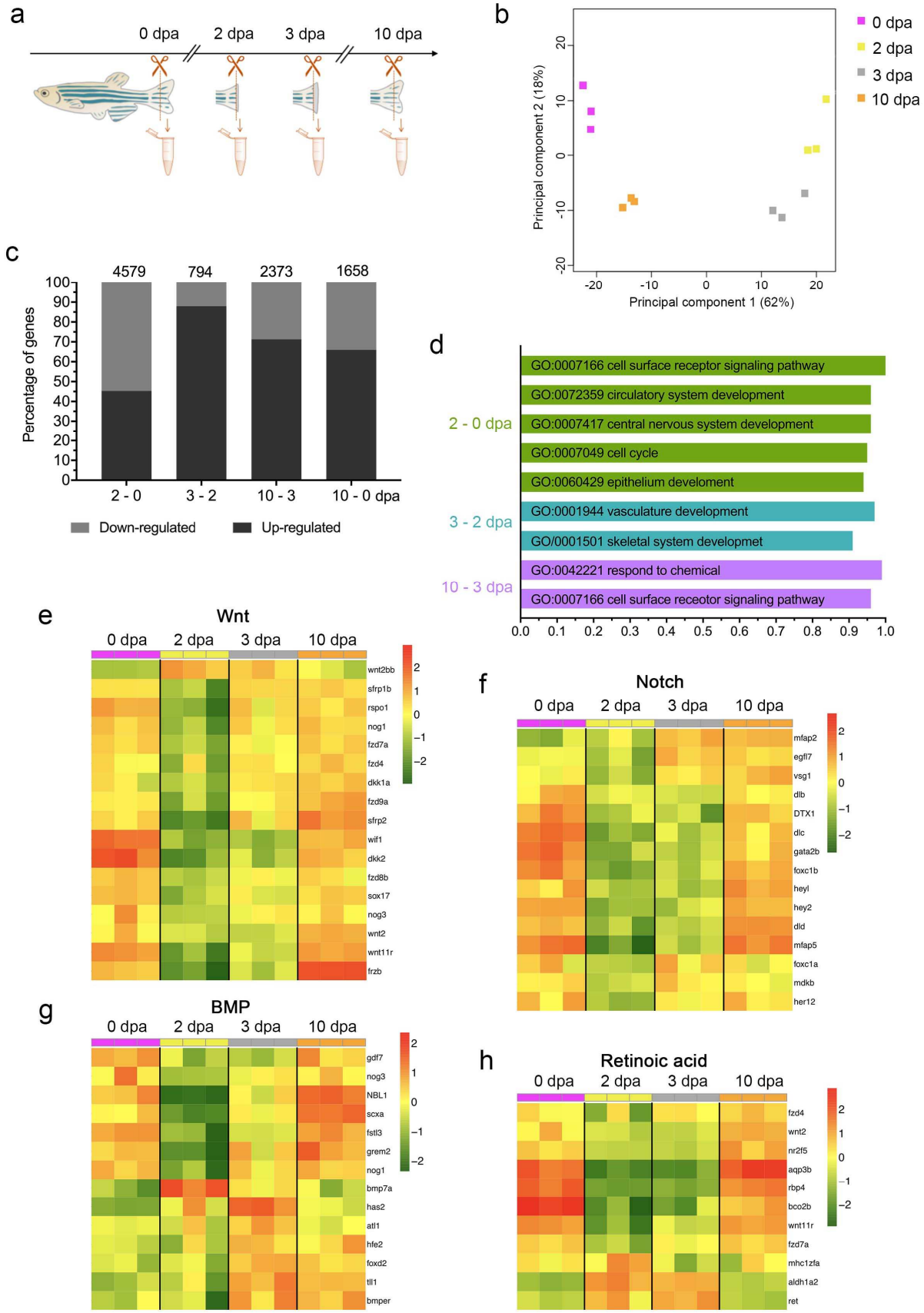
a
0 dpa
2 dpa
3 dpa
10 dpa
b
0 dpa
2 dpa
3 dpa
10 dpa
Principal component 2 (18%)
Principal component 1 (62%)
c
4579
794
2373
1658
Percentage of genes
2 - 0
3 - 2
10 - 3
10 - 0 dpa
Down-regulated
Up-regulated
d
2 - 0 dpa
3 - 2 dpa
10 - 3 dpa
GO:0007166 cell surface receptor signaling pathway
GO:0072359 circulatory system development
GO:0007417 central nervous system development
GO:0007049 cell cycle
GO:0060429 epithelium develoment
GO:0001944 vasculature development
GO/0001501 skeletal system developmet
GO:0042221 respond to chemical
GO:0007166 cell surface receotor signaling pathway
e
Wnt
wnt2bb
sfrp1b
rspo1
nog1
fzd7a
fzd4
dkk1a
fzd9a
sfrp2
wif1
dkk2
fzd8b
sox17
nog3
wnt2
wnt11r
frzb
f
Notch
mfap2
egfl7
vsg1
dlb
DTX1
dlc
gata2b
foxc1b
heyl
hey2
dld
mfap5
foxc1a
mdkb
her12
g
BMP
gdf7
nog3
NBL1
scxa
fstl3
grem2
nog1
bmp7a
has2
atl1
hfe2
foxd2
tll1
bmper
h
Retinoic acid
fzd4
wnt2
nr2f5
aqp3b
rbp4
bco2b
wnt11r
fzd7a
mhc1zfa
aldh1a2
ret

Figure 1. Overview of the gene regulation during zebrafish caudal fin regeneration. (a) Schematic representation of the RNA-seq time course experiment. A batch of six fish was used at each time point. The experiment was performed in triplicates. (b) Principal component analysis clustering based on the 1000 genes with the highest variance. Each point represents a biological replicate. Component 1 represents 62% of the variance and component 2 represents 18% of the variance. (c) Cumulative bar chart representing the percentage of downregulated (grey) or upregulated (black) genes normalized to 100 in the three conditions. Numbers on the top indicate the number of genes differentially expressed for each different comparison. q-values (corrected p-values) ≤ 0.1; fold-change ≥ 1. (d) Most represented GO terms in the different comparisons using a Model Based Gene Set Analysis (MGSA). x axis represents the scores. Only GO terms with score ≥ 0.90 were represented. MGSA parameters: false positive rate, α = 0.1; false negative rate, β = 0.77; number of active gene sets, p = 56. (e-h) Heatmaps illustrating differential expression of genes identified in the RNA-seq analysis and involved in Wnt (e), Notch (f), BMP (g) and Retinoic acid signaling pathways (h). Colors represent the intensity of the centered signal for each gene and gene names are given on the right. dpa: days post amputation.

Remarkably, most of the genes were differentially expressed between 0 dpa and 2 or 3 dpa while at 10 dpa, the latest time point analyzed, PCA analysis showed a tendency to progressively come back to the initial situation, at 0 dpa (Figure 1b). This is consistent with the fact that at 10 dpa, the appendage is macroscopically nearly restored and most of the fin structures are replaced (Figure S1) [3]. Bioinformatics analyses revealed that more than 4,500 genes are differentially expressed between 0 and 2 dpa, emphasizing important transcriptional rearrangements during this time period (Figure 1c). About 800 genes were also significantly regulated between 2 and 3 dpa suggesting active gene expression within this short time window, when the blastema is formed and the early regenerative outgrowth phase begins. Strikingly, most of the differentially regulated genes were downregulated at 2 dpa compared to 0 dpa whereas upregulated genes were predominantly observed at later stages (Figure 1c).

We then asked whether differentially regulated genes between the different time points represent specific Gene Ontology (GO) categories that can highlight differential biological activities in regenerating fins. The GO:0007166 ‘cell surface receptor signaling pathway’ was the most enriched

gene set in the 2-0 dpa interval (Figure 1d), illustrating the central role of communication between extra- and intracellular compartments during this time point interval. This short regeneration time period was also associated with the GO:0007049 'cell cycle' consistent with the high proliferation rate of blastemal cells during this period. Finally, the onset of tissue reconstruction was characterized by GO terms related to circulatory, central nervous and epithelium development between 0 and 2 dpa, and GO terms related to vasculature and skeletal system development between 2 and 3 dpa. It is consistent with our macroscopic observations showing that blood vessels form first and bones start to regenerate during the early phase of regrowth.

Next, we aimed at identifying signaling pathways differentially regulated during regeneration. We thus defined a gene set corresponding to the 500 most differentially expressed genes in the three following comparisons: 2-0 dpa (p-value ≤ 0.045 and 9.5 ≤ absolute fold change ≤ 260), 3-2 dpa (p-value ≤ 0.05 and 2.3 ≤ absolute fold change ≤ 76) and 10-3 dpa (p-value ≤ 0.048 and 5.1 ≤ absolute fold change ≤ 280); resulting in a group of 1097 gene after removing redundant genes. In our data, Wnt, Notch, BMP and Retinoic Acid signaling pathways were the most represented (Figure 1e-h, Figure S2a). Shh, FGFR and IGF1 signaling pathways also displayed significant number of differentially regulated genes (Figure S2). Heatmaps of the genes associated to the different pathways identified in our transcriptome, showed that genes of Wnt and BMP signaling pathways are the first ones to be re-activated at 3 dpa following a transient downregulation of all signaling pathways at 2 dpa (Figure 1e-h, Figure S2). This is consistent with the central role of Wnt signaling during zebrafish caudal fin regeneration that orchestrate the outgrowth *via* secondary signals. Most of these secondary signaling pathways that have been reported to regulate blastemal cell proliferation, osteoblasts maintenance and differentiation and epidermal patterning during fin regeneration [17] were also identified in our transcriptome; *i.e.* BMP, Notch, Retinoic Acid, IGF, Hedgehog, FGFR (Figure S2).

We then analyzed the GO terms related to Cellular Process (GO:0009987) using two different approaches: the hypergeometric method and the Model-based Gene Set Analysis. Strikingly, GO:0043062 "extracellular structure organization" and GO:0022617 "extracellular matrix disassembly" were the most represented, underscoring the fundamental role of ECM during regeneration (Table S1). The enrichment of GO terms related to 'cell-cell signaling' (GO:0007267) and 'G-coupled receptors signaling pathways' (GO:0007186) were also observed (Table S1). Our data underscore the role of ECM in regeneration.

2.2. Kinetic of basement membrane gene expression during regeneration recapitulates BM embryonic development

Different BMs are present in caudal fins: between the epidermis and dermis, around nerves and blood vessels. As epidermis closure is the first step of fin regeneration, the first BM to be formed is the epidermal one. The current model of BM structure assumes that BM consists of two layers formed by distinct self-assembling protein networks made of laminins and collagen IV, respectively. The inner laminin and outer collagen IV networks are linked through interactions with nidogen and perlecan. Thus, we next analyzed our transcriptome data using the proteomic definition of the BM [10] and the *in-silico* zebrafish matrisome database [11], we determined the kinetics of BM gene expression during fin regeneration (Table S2).

Among the BM toolkit genes, laminin genes were the first to be upregulated during caudal fin regeneration, in particular the *lama5*, *lamb1a* and *lamc1* genes, encoding laminin 511, a laminin reported to be required for skin integrity in developing zebrafish [18] (Figure 2a, Table S2). In contrast, *lamb1b* was downregulated during the same time period consistently with previous data showing that *lamb1a* but not its paralogue is necessary for the maintenance of basal epithelial cell polarization after fin amputation [19]. Interestingly, Collagen IV encoding genes were then expressed, at 3 and 10 dpa (Figure 2b, Table S2) indicating that the formation of the two BM layers during regeneration recapitulates the scenario described for BM development, with laminin deposition first and collagen IV in a second time [8]. Genes of the Fraser complex, which are early required for the dermo-epidermal cohesion during mammalian embryonic development [20], were consistently highly upregulated between 0 and 2 dpa (Figure 2c, Table S2).

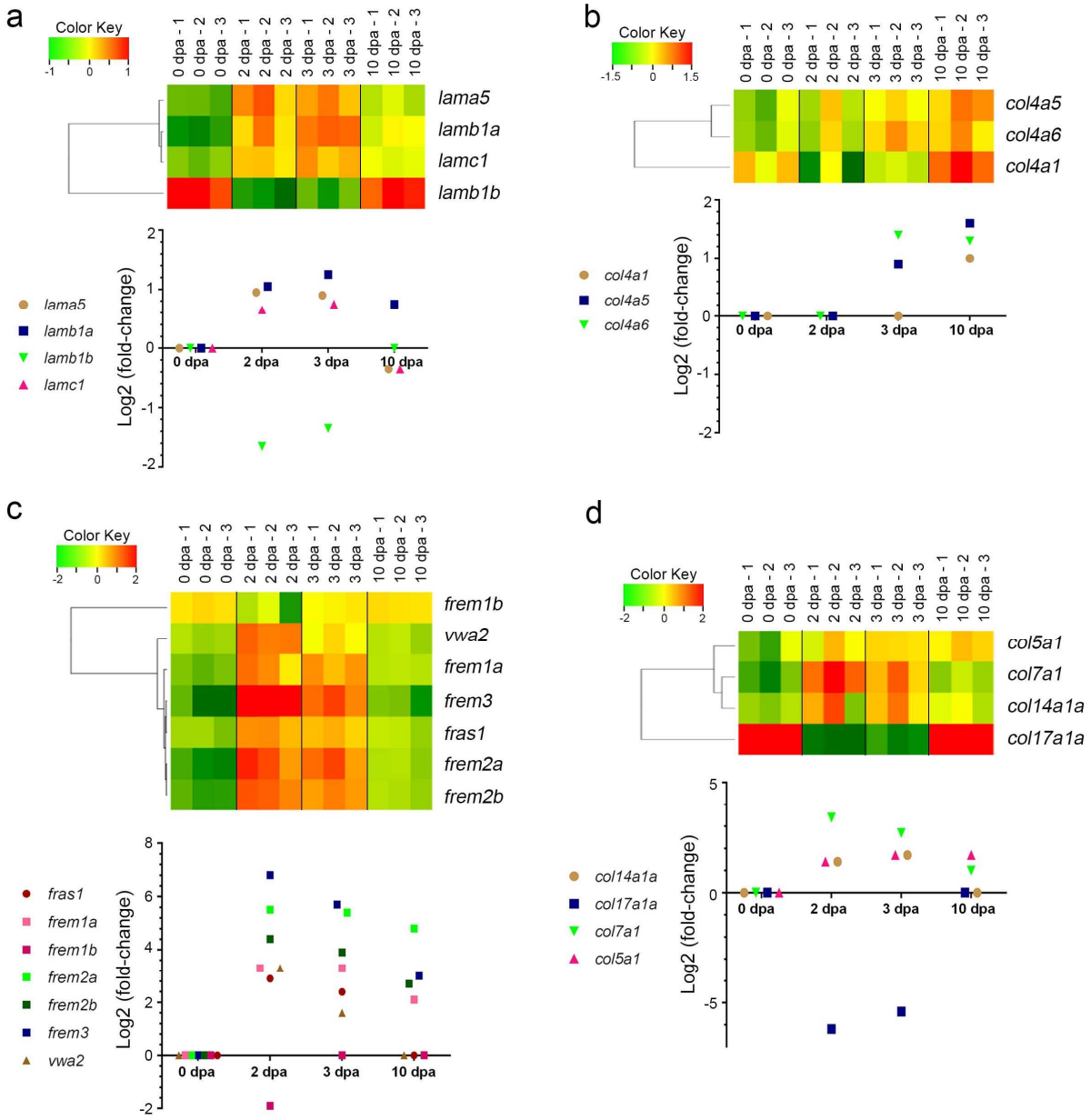

Figure 2. Basement membrane gene expression during fin reconstruction. For each panel (a - d), heatmaps illustrating differential expression of some basement membrane genes for each replicate at different time points of regeneration (upper) and corresponding dot plots (lower). (a) Laminin 511 encoding genes are represented. (b) Collagen IV network encoding genes are represented. (c) Fras1/Frem complex encoding genes are represented. (d) Collagen of the basement membrane zone (except collagen IV) encoding genes are represented. Colors represent the intensity of the centered signal for each gene. dpa: days post amputation.

Apart from the BM toolkit genes, BM-associated collagen genes were also tunely regulated during regeneration. Specifically, *col17a1a*, the functional orthologue of the mammalian collagen XVII [21], was strongly downregulated at the beginning of tissue reconstruction (Figure 2d, Table S2). Collagen XVII is a structural component of hemidesmosomes, a multiprotein complex located at the dermo-epidermal BM zone that anchors the basal epithelial layer to the BM in mammalians [22,23]. This is in accordance with the absence of hemidesmosome-like structures in the regenerating caudal fin at 3 dpa as observed by transmission electron microscopy (TEM) (Figure S3). Expression of *col7a1*, encoding collagen VII, the major component of anchoring fibrils at the dermo-epidermal junction zone, peaked at 2 dpa and was then progressively downregulated at later stages. Interestingly, the BMZ collagen, *col14a1a,* was also found transiently upregulated at 2 and 3 dpa as observed for laminins. Collagen XIV is a poorly characterized ECM component though ColXIV-A was accepted as an intrinsic component of specialized basement membrane zones in zebrafish [12]. Zebrafish possesses two human *COL14A1* orthologues, *col14a1a* and *col14a1b* [12]. However, *col14a1b* was not observed in our transcriptome, a result confirmed by RT-qPCR (Figure 4c), indicating that *col14a1a* is the only paralogue involved in regeneration. Transient expression of *col14a1a* was confined to proliferative epithelia in developing embryo and expression dropped after hatching though the protein lasted in the BM at later stages (Figure 3) [12].

To confirm at the protein level the specific re-expression during regeneration of the main components of the BMZ, we performed double staining of regenerating caudal fin at 3 dpa when BMZ proteins should be deposited in the regenerating BM. Double staining of transversal or longitudinal sections of regenerating fins at 3 dpa with an anti-pan-Laminin and our antibodies against ColXIV-A [12] (Figure 3a) revealed that ColXIV-A co-localized with the laminin-stained basement membrane underlying the basal cells of epidermis (Figure 3b). At the confocal resolution, ColXIV-A also co-localized with ColIV network that forms the outside layer of the epidermal BM (Figure 3c). According to our transcriptomic analysis, the Fraser complex encoding genes were re-expressed during zebrafish caudal fin regeneration and exhibited a clear kinetic correlation with *col14a1a* gene expression (Figure 2c, d). Sections were thus double stained with antibodies against ColXIV-A and Amaco, a newly identified component of the Fraser complex [24,25] encoded by *vwa2* and showed that the two proteins co-localized in the BMZ at 3 dpa (Figure 3d). Our data at the protein level nicely coincided with our time-course transcriptional profiling of regenerating caudal fin (Figure 2). Taken together our data showed

that kinetics of BM gene expression during caudal fin regeneration follows the “regeneration recaps development” popular paradigm.

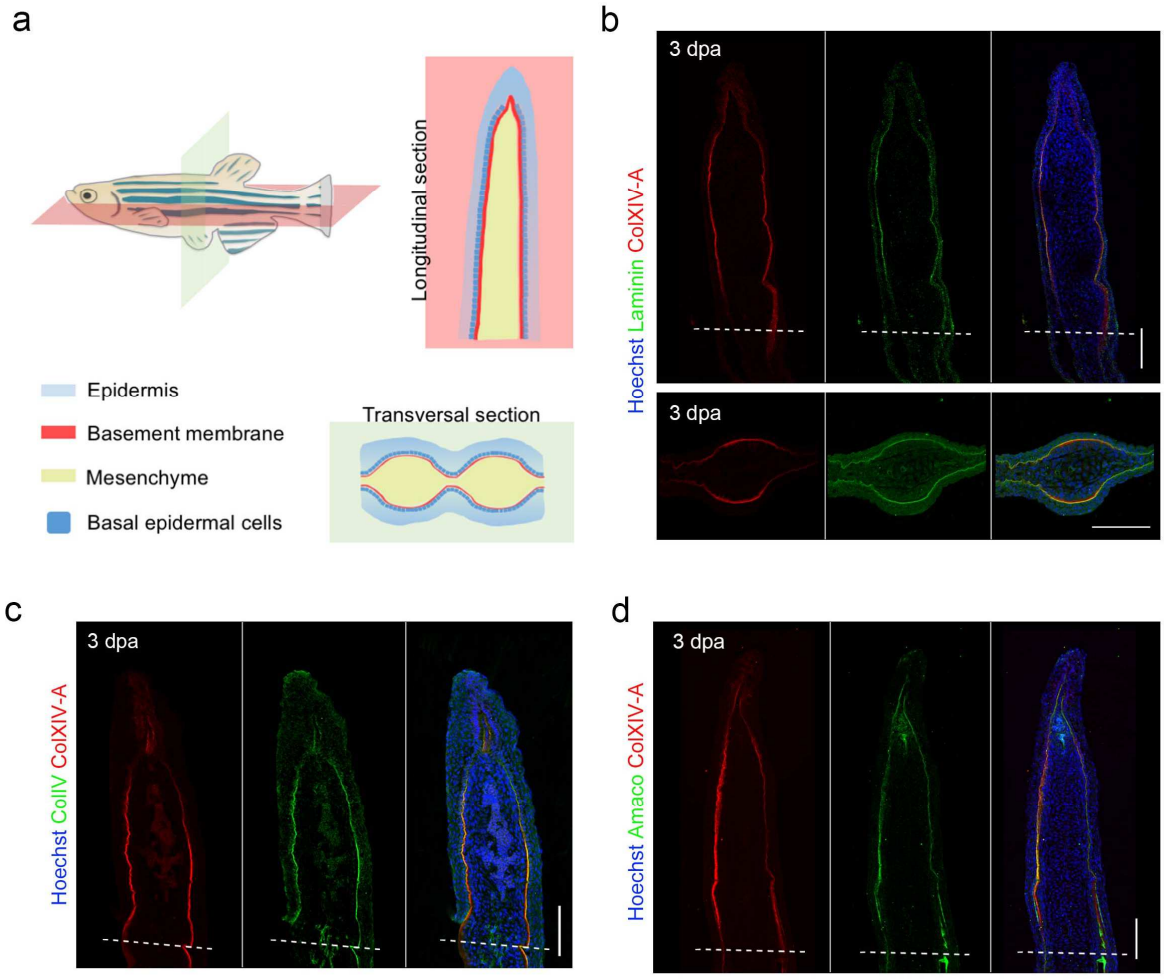

Figure 3. Immunostaining of the basement membrane components during fin regeneration. (a) Schematic representation of the zebrafish longitudinal and transversal section planes (upper left) and of the tissue organization on sections (right). (b) Immunofluorescent staining on fin longitudinal (upper) and transversal (lower) sections at 3 dpa with anti-ColXIV-A (red) and anti-Laminin (green) antibodies. (c) Immunofluorescent staining on fin longitudinal sections at 3 dpa with anti-ColXIV-A (red) and anti-ColIV (green) antibodies. (d) Immunofluorescent staining on fin longitudinal sections at 3 dpa with anti-ColXIV-A (red) and anti-Amaco (green) antibodies. (a-d) Nuclei are stained in blue. Merged images are on the right. Scale bars: 100 µm. Dotted lines indicate the amputation site. dpa: days post amputation.

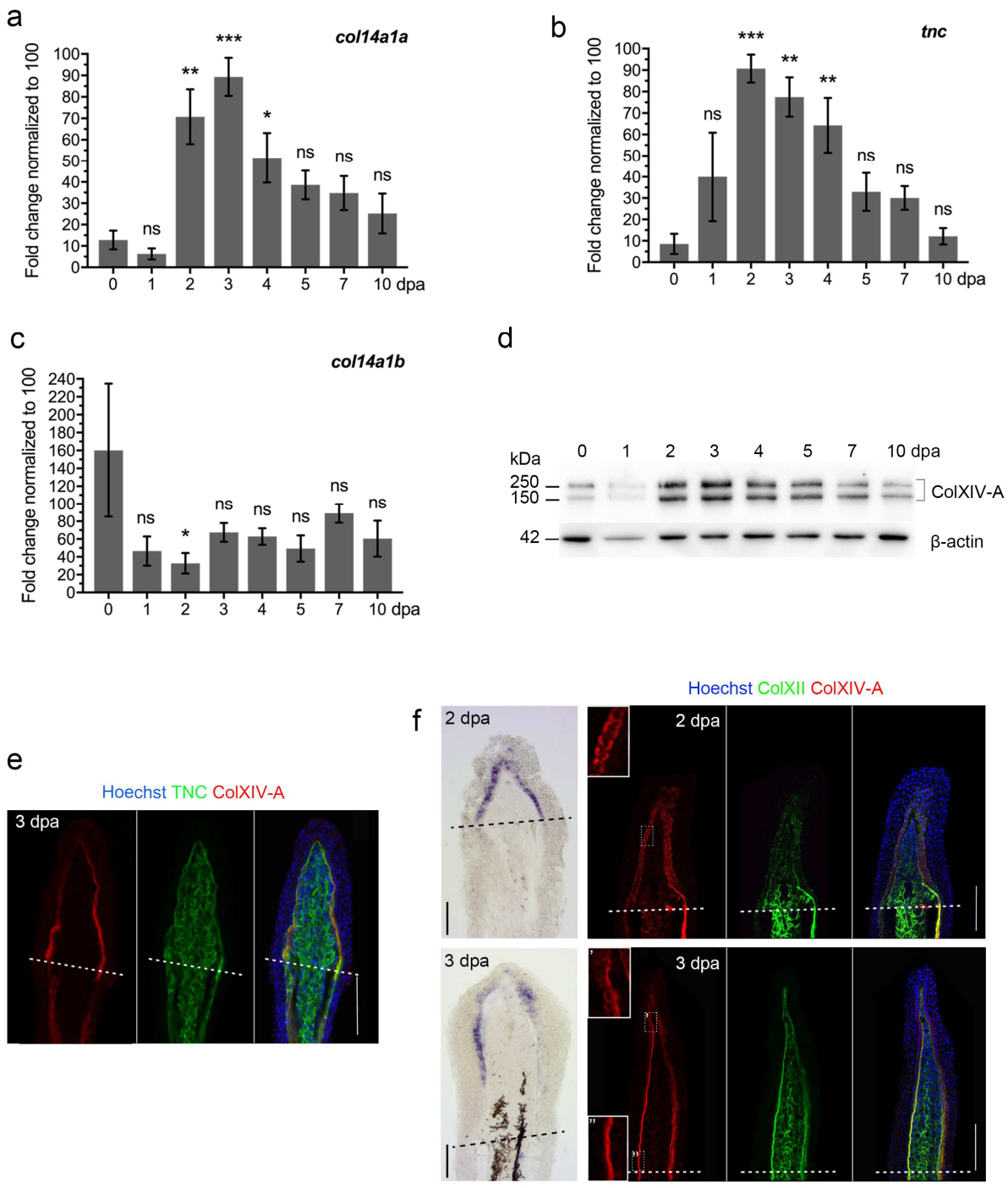

*Figure 4. Expression and distribution of specific genes upregulated at early blastema stage during fin regeneration. (a-c) Bar chart representing RT-qPCR analysis of col14a1a (a), tnc (b) and col14a1b (c) mRNA expression during caudal fin regeneration. For each gene the maximal expression of each replicate during regeneration was normalized to 100%. Asterisks indicate p-values: ***≤0.001, **≤0.01, *≤0.05, ns: non-significant. (n=3). (d) Western blot with anti-ColXIV-A antibodies on total protein extracts during caudal fin regeneration. ColXIV-A lower bands correspond to monomer, upper*

bands to dimer (brackets). β-actin was used as a loading control. Molecular weights (in kDa) are indicated on the left. Data shown are one representative experiment among three replicates. (e) Immunofluorescence staining of fin longitudinal sections at 3 dpa with anti-ColXIV-A (red) and anti-TNC (green) antibodies. (f) Left: in situ hybridization with col14a1a specific probe of longitudinal sections of regenerating fins at 2 dpa (upper panel) or 3 dpa (lower panel). Right: Immunofluorescence staining of fin longitudinal sections at 2 dpa (upper panel) or 3 dpa (lower panel) with anti-ColXIV-A (red) and anti-ColXII (green). (e-f) Nuclei are stained in blue. Merged images are on the right. Dotted lines indicate the amputation site. dpa: days post amputation. Scale bars: 100 µm.

2.3. col14a1a is part of the regeneration-specific gene program

The induction of *col14a1a* in the basal epithelial layer during development [12] and during regeneration (Figure 2d) strongly suggested a role for ColXIV-A in creating the BM structure. We thus further detailed its expression profile at the transcript and protein levels using RT-qPCR (Figure 4a) and Western blot (Figure 4d) respectively during early and late phases of regeneration. We showed that induction of *col14a1a* gene expression occurred at the onset of blastema formation between 1 and 2 dpa and expression sharply peaked at 2-3 dpa and then decreased progressively to reach its initial level at 10 dpa (Figure 4a), following a gene expression kinetic consistent with the protein expression pattern (Figure 4d). Interestingly, gene expression kinetics of *col14a1a* and *tnc*, encoding Tenascin C a marker of regeneration and wound healing expressed by mesenchymal cells [26] were highly similar (Figure 4a and b) even though fold changes were variable (Figure S4a-c) . Although gene expression kinetics of *col14a1a* and *tnc* were similar, double immunostaining showed that the two protein expression domains in the fin were distinct: ColXIV-A underlined the epidermis and Tenascin C demarcated the mesenchymal tissue at 3 dpa (Figure 4e).

We then further detailed the *col14a1a* expression and ColXIV-A precise localization in regenerative fin. We previously reported that *col14a1a* is specifically expressed in proliferative epithelia in developing embryo [12]. *In situ* hybridizations of regenerating fins showed that *col14a1a* mRNA is expressed by proliferative epidermal basal cells of the outgrowth at 2 and 3 dpa (Figure 4f). At 3 dpa, *col14a1a* expression was restricted to the distal part of outgrowth as fin regrows, consistent with *col14a1a* expression pattern in embryo. Immunostaining of regenerating fins showed intracellular ColXIV-A in the basal epidermal cells of the outgrowth at 2 dpa that is progressively deposited in the

BMZ from the proximal to the distal part of the regenerate (Figure 4f, Figure S4d). Intracellular ColXIV-A was clearly present in the distal part of the regenerate at 3 dpa whereas it was only barely observed in the proximal part indicating that the protein has already been deposited in the extracellular space as a thin sheetlike structure. Collagen XII (ColXII) which is closely related to ColXIV-A showed a complementary location with ColXIV-A in developing appendages: ColXIV-A underlined epidermal BM while ColXII demarcated the mesenchymal tissue [12]. In the regenerating fin, ColXII is found in basal epithelial cells at 2 dpa but expression strictly switched to mesenchymal cells at 3 dpa (Figure 4f). We conclude that ColXIV-A expression is temporally and spatially controlled during regeneration and thereby is part of the regeneration-specific gene program.

2.4. Lack of ColXIV-A impairs laminin deposition in regenerative BM

To investigate the role of ColXIV-A in the organization of BMZ and/or at the tissue interface, we generated a *col14a1a* CRISPR/Cas9 knockout line. A 4 nucleotides deletion mutation leading to a disruption of the reading frame was selected (Figure S5a and b). As demonstrated by western blot and immunofluorescence, *col14a1a*$^{-/-}$ fish showed a complete absence of ColXIV-A at 72 hours post fertilization (Figure S5c and d) and in 3 dpa regenerating adult fins (Figure 5a and Figure S5e). Quantification of ColXIV-A amount in heterozygous fish showed a decrease of 60% compared to WT (Figure 5a and Figure S5c). *col14a1a*$^{-/-}$ embryos developed normally, adults were fertile and lack of ColXIV-A did not impair caudal fin regrowth after amputation (Figure S6). Changes in BM composition can affect cell proliferation, migration and differentiation [27]. Staining of 3 dpa *col14a1a*$^{-/-}$ fin outgrowth with antibodies against p63, a marker of epithelial proliferation showed that lack of ColXIV-A did not affect epithelial cell proliferation nor the columnar/cuboid epithelial cell organization (Figure S7a). Similarly, immunostaining with ECM markers of regenerating mesenchyme, Collagen I, Tenascin C and Collagen XII, were similar in 3 dpa WT and *col14a1a*$^{-/-}$ fins (Figure S7b-d).

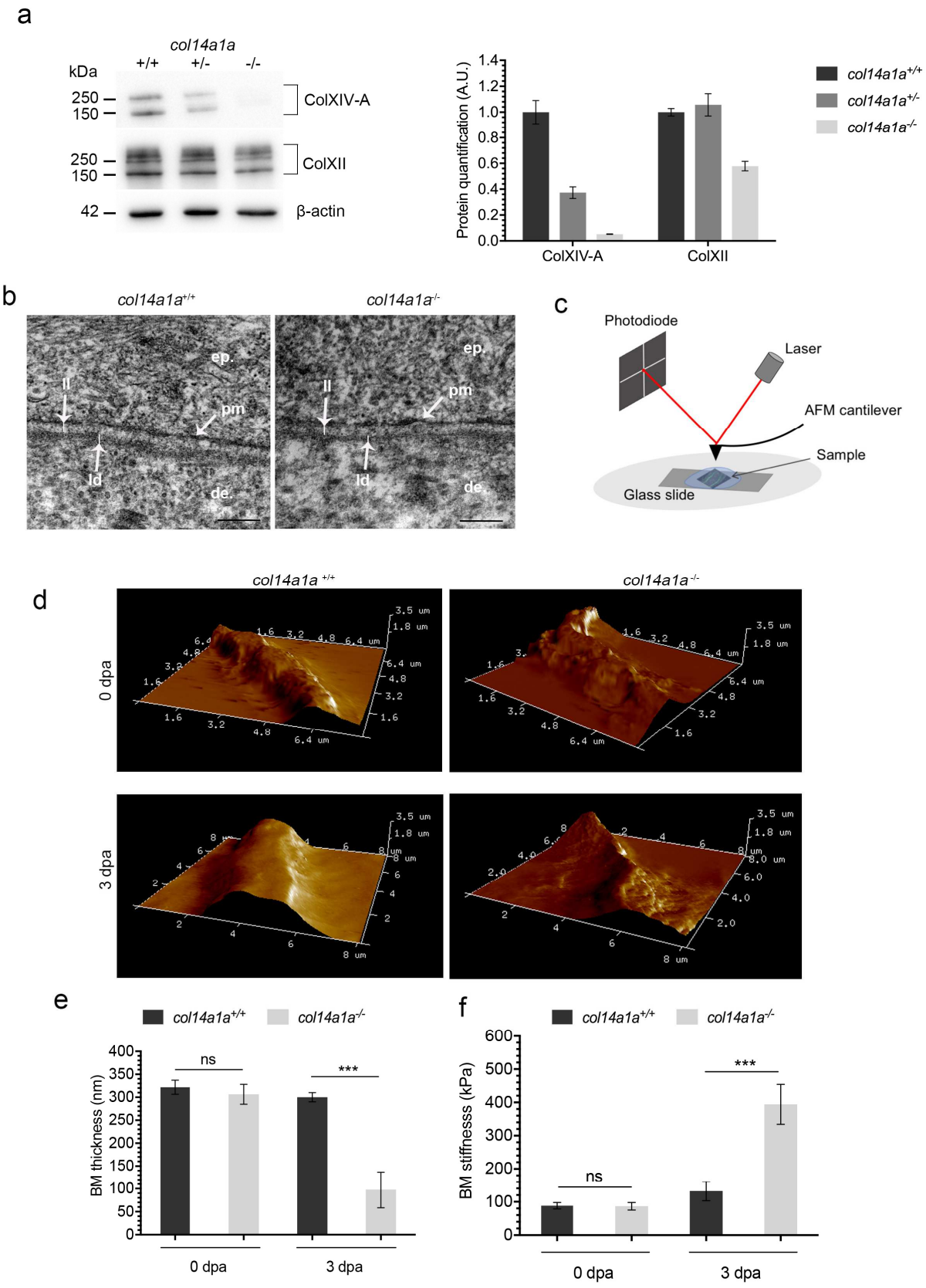
a
col14a1a
+/+
+/-
-/-
kDa
250
150
ColXIV-A
250
150
ColXII
42
β-actin
Protein quantification (A.U.)
col14a1a+/+
col14a1a+/-
col14a1a-/-
ColXIV-A
ColXII
b
col14a1a+/+
col14a1a-/-
ep.
ll
pm
ld
de.
c
Photodiode
Laser
AFM cantilever
Sample
Glass slide
d
col14a1a +/+
col14a1a -/-
0 dpa
3 dpa
e
col14a1a+/+
col14a1a-/-
BM thickness (nm)
ns
***
0 dpa
3 dpa
f
col14a1a+/+
col14a1a-/-
BM stiffness (kPa)
ns
***
0 dpa
3 dpa

*Figure 5. ColXIV-A inactivation leads to basement membrane mechanical defects during regeneration. (a) Right: western blot with anti-ColXIV-A and anti-ColXII antibodies on total protein extracts of col14a1a$^{+/+}$, col14a1a$^{+/-}$ and col14a1a$^{-/-}$ fish at 3 dpa. β-actin was used as a loading control. ColXIV-A and ColXII lower bands correspond to monomer, upper band to dimer (brackets). Molecular weights (in kDa) are indicated on the left. Data shown are one representative experiment among three replicates. Left: bar chart representing densitometric quantification of relative ColXIV-A and ColXII expression levels normalized to β-actin. A.U.: Arbitrary Units. (b) Transmission electron microscopy images of col14a1a$^{+/+}$ and col14a1a$^{-/-}$ regenerating fins at 3 dpa. Brackets indicate basement membrane. ep.: epidermis, de.: dermis. Scale bars: 200 nm. (c) Schematic representation of the atomic force microscopy experiment protocol. (d) Surface topography images of col14a1a$^{+/+}$ (left) and col14a1a$^{-/-}$ (right) at 0 dpa (upper) and 3 dpa (lower) obtained by atomic force microscopy. Reliefs represent basement membrane and flat parts represent the tissue around. (e-f) Bar chart representing basement membrane thickness (e) or stiffness (f) of col14a1a$^{+/+}$ and col14a1a$^{-/-}$ at 0 and 3 dpa measured by atomic force microscopy. Asterisks indicate p-values: ***≤0.001; ns: non significant. (n = 3). dpa: days post amputation.*

ColXIV-A morpholino knock-down in embryos resulted in defective epidermis anchorage to the underlying mesenchymal tissue, even though its absence did not cause skin blisters [12]. This was not observed in *col14a1a*$^{-/-}$ non-amputated adult fins and in regenerating fins (data not shown). We thus analyzed whether the absence of ColXIV-A alters the deposition or organization of BM components during its regeneration though causing a subtler phenotype. At 2 dpa, the Fraser complex protein Amaco was present in the BM zone of both WT and *col14a1a*$^{-/-}$ outgrowth except at the very tip (Figure 6a). At 3dpa, WT and *col14a1a*$^{-/-}$ BM stained as a continuous line with antibodies to Amaco and collagen IV (Figure 6b and c). In contrast, laminins deposition was markedly altered in 3 dpa *col14a1a*$^{-/-}$ fish compared to WT (Figure 6d). In absence of ColXIV-A, we observed that laminins accumulated in intracellular compartments of basal epidermal cells and no extracellular protein deposition was visible whereas BM appeared as a continuous intensely stained fine line in controls (Figure 6d). The laminin phenotype was observable in a short window of time. Although *lam transcripts* were expressed at 2dpa (Figure 2a), laminin immunoreactivity was not yet detected at 2 dpa neither in *col14a1a*$^{-/-}$ nor WT regenerating BM (Figure 7a). This may be a particular feature of

laminin synthesis since Amaco which transcripts are expressed at 2 dpa, was already detectable in the basement membrane at 2 dpa (Figure 7b). At 4 dpa, deposition of laminins in the *col14a1a*$^{-/-}$ BM was similar to WT and signals merged with ColIV immunoreactivity (Figure 7c and d).Deposition of ColXIV-A and laminins in the extracellular space appeared to be inter-dependent and might involve similar mechanisms. The defect in laminins deposition did not seem to affect normal collagen IV deposition in the BM at the confocal resolution at 3 dpa or 4 dpa (Figure 6c and Figure 7c). Accordingly, TEM of 3 dpa *col14a1a*$^{-/-}$ regenerating fins showed that BM is thinner than in WT, although it displayed the characteristic sheet-like structure of BM (Figure 5b, Figure S8). Quantification of TEM images showed that the lamina densa but the lamina lucida is thinner in *col14a1a*$^{-/-}$ fins compared to WT. This is in accordance with the fact that the lamina lucida is a known artifact due to the conventional TEM method of tissue preparation that includes dehydration steps (Figure S8) [28]. We conclude that ColXIV-A is involved in the organization of the BM during its formation and contributes to proper and timely deposition of laminins suggesting that ColXIV-A helped laminins integration within the regenerative BM.

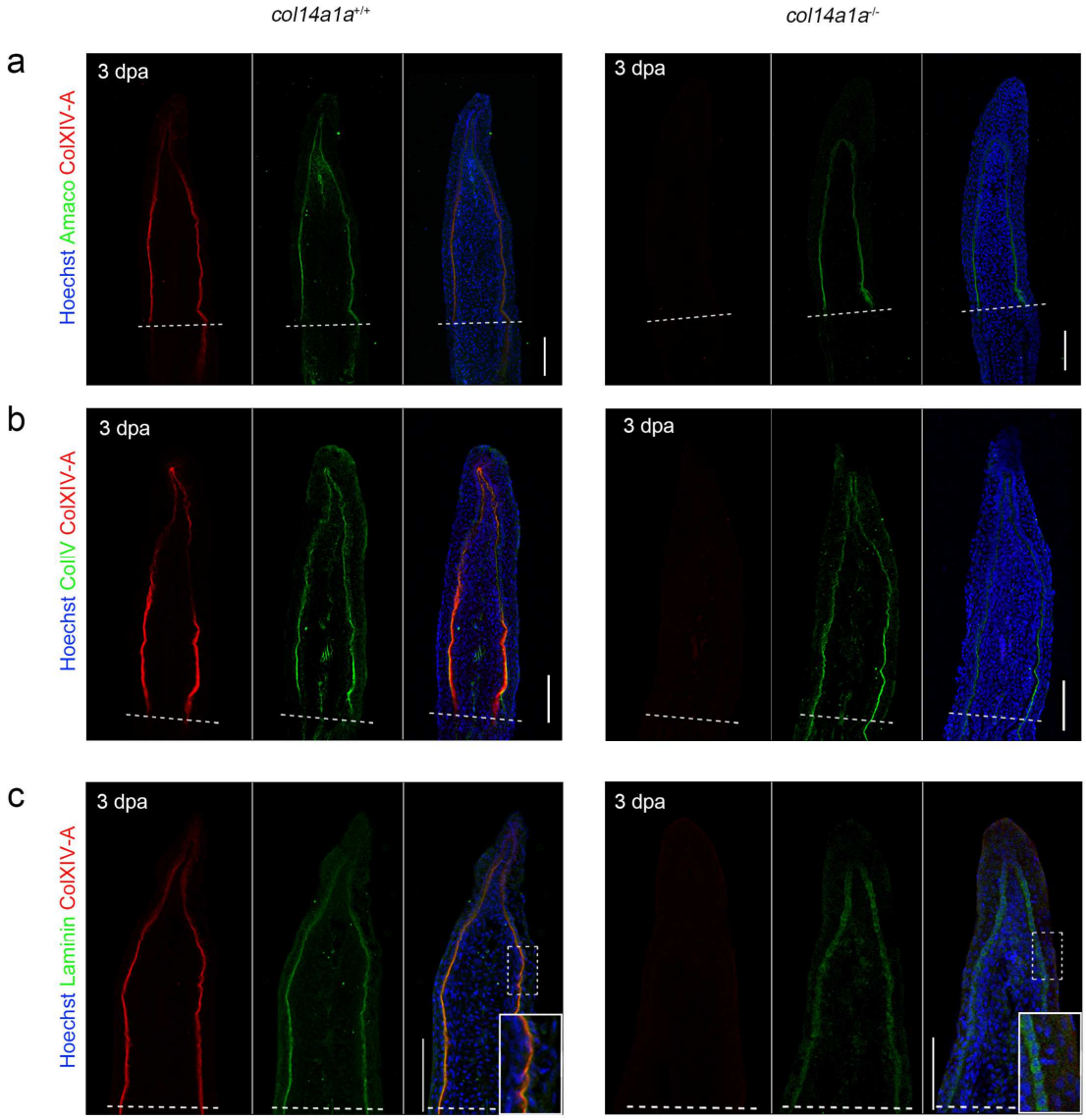

Figure 6. ColXIV-A invalidation delayed laminins deposition in the reconstructing basement membrane. Immunofluorescent staining of col14a1a$^{+/+}$ (left) or col14a1a$^{-/-}$ (right) fin longitudinal sections at 3 dpa with anti-ColXIV-A (a-c, red) and anti-Amaco (a, green), anti-ColIV (c, green) and anti-pan-Laminin (d, green) antibodies. n=5/6. (a-d) Nuclei are in blue. Merged images are on the right. Dotted lines indicate the amputation site. dpa: days post amputation. Scale bars: 100 µm.

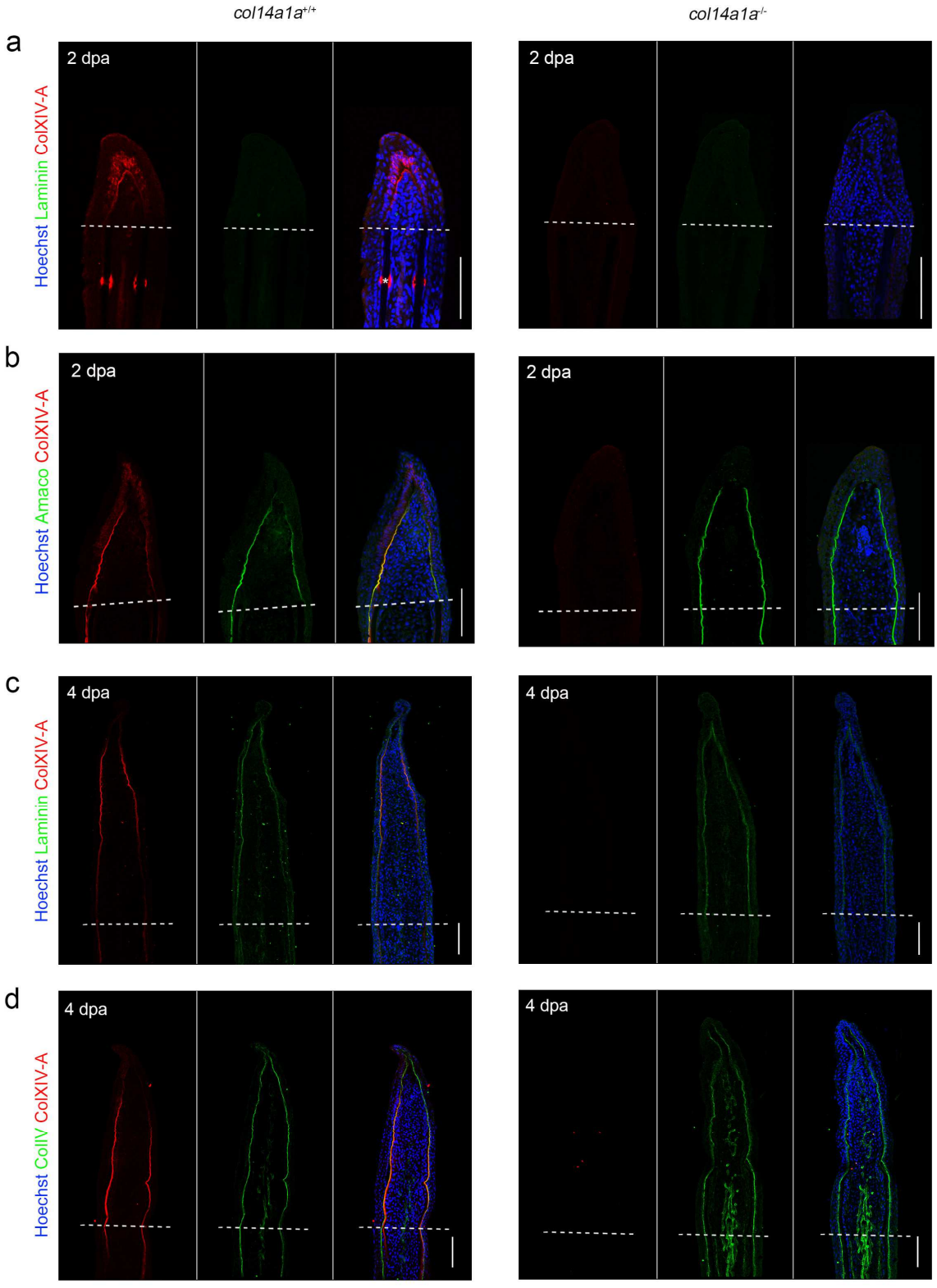

Figure 7. Deposition of laminin in the basement membrane of caudal fin skin at 2 dpa and 4 dpa. Immunofluorescence co-staining of caudal fin longitudinal sections with anti-ColXIV-A (a-c, red) and anti-pan-Laminin (a and c, green) or anti-Amaco (b, green) or anti-ColIV (d, green). Nuclei are in blue. Merged images are on the right. Dotted lines indicate the amputation site. Asterisk points to ColXIV-A

staining at the segmental borders (ligament) of bony rays in the stump. dpa: days post amputation. Scale bars: 100 µm.

2.5. ColXIV-A is a molecular regulator of BM structure and biomechanics during fin regeneration

Changes in the structural organization of BM can affect its mechanical properties. To address this question we used AFM, a standard approach to measure the elastic modulus of biological samples, coupled with epifluorescence microscopy to accurately locate the epidermal BM. Frozen sections of *col14a1a*$^{-/-}$ and WT regenerating fins were thus stained with anti-panLaminins before AFM analysis (Figure 5c). Topography images revealed that BM is a solid and rigid structure, thus imaged as a three-dimensional relief, compared to the surrounding soft material (Figure 5d). The elastic modulus quantifies how easily an elastic material is deformed when a force is applied to it; a high value of elastic modulus thus corresponds to a stiff sample. Measurements of thickness and stiffness of epidermal BM before amputation gave similar results in WT and *col14a1a*$^{-/-}$ (Figure 5e and f – 0 dpa, Table S3). In striking contrast, AFM measurements and topographic images showed that regenerating epidermal BM of *col14a1a*$^{-/-}$ fish at 3 dpa was significantly thinner compared to non-amputated fins (Figure 5d and e, Table S3). Decreased in thickness was accompanied by a substantial increase in the stiffness of *col14a1a*$^{-/-}$ epidermal BM compared to WT (Figure 5f, Table S3). Recovery of the initial values at later stages indicated a transient role of ColXIV-A in BM assembly and organization (data not shown).

To confirm this result, we performed *vivo*-MO knockdown to block *col14a1a* expression in regenerating WT adult fins. Translation blocking *vivo*-MO against *col14a1a* or 5 bp mismatch controls (*vivo*-MS) were injected in the dorsal half of 2 dpa fins whereas the uninjected ventral part served as control, as previously described [29] (Figure S9a). The efficiency and specificity of ColXIV-A knockdown were assessed with immunostaining and western blot at 3 dpa corresponding to 1 day post-injection (dpi) (Figure S9b and c). In agreement with the results obtained with *col14a1a*$^{-/-}$ fish, TEM showed that the epidermal BM of *vivo*-MO-injected fins was significantly thinner than in MS controls (Figure S9d). Accordingly, AFM analysis of 1 dpi *vivo*-MO and *vivo*-MS-injected fins confirmed that lack of ColXIV-A impairs proper regeneration of the BM and results in the formation of a thinner and stiffer structure (Figure S9e and f, 230±50 nm; 815±163 kPa and 314±40 nm; 284±12

kPa for *vivo*-MO- and *vivo*-MS-injected fins respectively). We conclude that ColXIV-A is required for the organization and physical properties of epidermal BM during regeneration.

2.6. ColXIV-A acts as a molecular spacer required for proper shaping and biomechanics of BM

To refine the role of ColXIV-A in the organization of the regenerating BM, we next performed stiffness tomography experiments at the nanoscale level. To be able to distinguish structures of different stiffness throughout the BM thickness, the atomic force microscope has been operated as a nano-indenter to gather the deformation of the cantilever as a function of the depth as described [30]. An array of 10 by 10 measurements was acquired for each sample and the elastic modulus was extracted at various depths (Figure 8a and b).

Reconstructions of non-amputated WT BM sections (0 dpa) stunningly revealed a checkerboard pattern made of highly stiff areas and soft material. The stiff areas of about 130-190 kPa likely corresponded to structural protein networks (laminins and/or collagen IV) and the soft regions of about 30-50 nm represented regions rich in small molecules or water (Figure 8c, left). Similar profiles were observed in non-amputated *col14a1a*$^{-/-}$ fins (0 dpa) (Figure 8c, right) and in WT at 3 dpa (Figure 8d, left) with highest and lowest values in the same range. In striking contrast, the epidermal BM profile of 3 dpa *col14a1a*$^{-/-}$ fins displayed a complete different pattern in which the soft regions were nearly absent (Figure 8d, right). The maximum stiffness increased by 220% in 3 dpa *col14a1a*$^{-/-}$ fins (422 kPa) compared to WT (191 kPa). As such, the BM of *col14a1a*$^{-/-}$ regenerating fins appeared as a very compact structure. In conclusion, we have shown that the three-dimensional structure of BM at the nanoscale level is remarkably organized in a checkerboard pattern. Lack of ColXIV-A altered the regenerating BM three-dimensional organization and ultimately its biomechanics. ColXIV-A is a FACIT collagen. Members of this subset of the collagen superfamily play central roles in the formation of complex regulatory networks to execute various functions [31]. We thus conclude that ColXIV-A acts as a molecular spacer to regulate proper organization and biomechanics of regenerating BM, as illustrated in Figure S10.

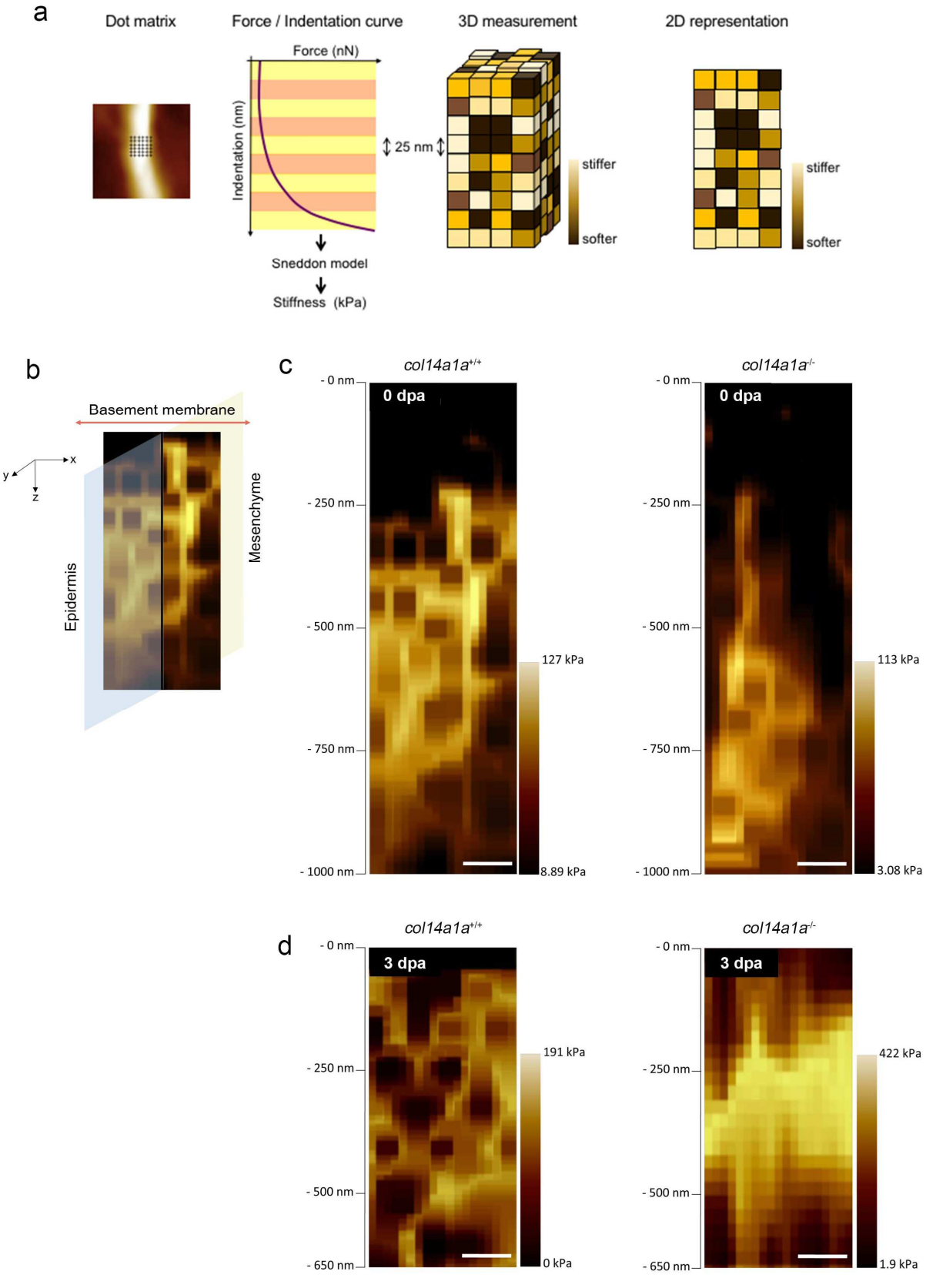
a
Dot matrix
Force / Indentation curve
3D measurement
2D representation
Force (nN)
Indentation (nm)
25 nm
Sneddon model
Stiffness (kPa)
stiffer
softer
stiffer
softer
b
Basement membrane
x
y
z
Epidermis
Mesenchyme
c
col14a1a+/+
col14a1a-/-
0 dpa
0 dpa
- 0 nm
- 250 nm
- 500 nm
- 750 nm
- 1000 nm
127 kPa
8.89 kPa
113 kPa
3.08 kPa
d
col14a1a+/+
col14a1a-/-
3 dpa
3 dpa
- 0 nm
- 250 nm
- 500 nm
- 650 nm
191 kPa
0 kPa
422 kPa
1.9 kPa

Figure 8: ColXIV-A invalidation impacts the regenerating basement membrane biomechanics. (a) Schematic representation of the stiffness tomography experiment. A 10 x10 matrix of force-indentation curves was obtained for each basement membrane analyzed. For each force-indentation curve the Sneddon model is applied in order to extract the elastic modulus (stiffness). This information is used to construct a 3D stiffness profile of the sample as a function of penetration depth (z-position). Projection images were used for illustration. (b) Schematic representation of the samples orientation during tomography measurements. (c-d) 2D tomography images of the basement membrane of col14a1a$^{+/+}$ (left) and col14a1a$^{-/-}$ (right) at 0 dpa (c) or 3 dpa (d). Numbers on the left indicate relative depth inside the tissue. Color code indicates stiffness of the matrix from softer regions (dark brown) to stiffer regions (light yellow). Scale bars: 100 nm. dpa: days post amputation.

3. Discussion

Our transcriptomic analyses first provided a current evidence for a critical role of the ECM in tissue regeneration since the most enriched gene sets in our study were related to it [26,32,33]. More interestingly, our global approach revealed that the BM gene expression profiling observed across the regenerative time course follows the “regeneration recaps development” paradigm. As such, laminin genes were expressed earlier than collagen IV genes as in development [34]. Consistently, we observed the re-expression of genes whose expression was restricted to the embryonic development of BM, such as genes encoding the Fraser complex [35] and *col14a1a* [12]. Gene expression kinetics and expression patterns of Amaco and ColXIV-A were strikingly superimposable showing a peak of transcript levels and protein colocalization at the BMZ between 2 dpa and 3 dpa suggesting a possible physical interaction between the two proteins. Unlike Fraser complex genes mutants which all carried null mutations [18,36], Amaco knockdown in zebrafish developing embryos did not result in skin blistering phenotype but increased the phenotype of Fras 1 hypomorphic zebrafish embryos [24]. ColXIV-A knockdown or genetic invalidation also did not dramatically affect the development of the zebrafish embryo suggesting an even subtler phenotype. ColXIV-A could be a new component of the Fraser complex or at least physically interact with it. A possible synergistic interaction between *fras1* and *col14a1a* will be further investigated to address this question.

Concomitantly with zebrafish embryogenesis [12], *col14a1a* is specifically expressed in a short time window by highly proliferative epithelia during adult caudal fin regeneration. *col14a1b* was not differentially expressed during caudal fin regeneration, excluding a possible redundancy between the two paralogues. This is consistent with the fact that paralogue specification following the teleost-specific whole genome duplication is a common phenomenon, as already shown for collagen genes during both zebrafish development and regeneration (Duran *et al.*, 2015, Pagnon-Minot *et al.*, 2008; Bretaud *et al.*, 2011; Guillon, Bretaud and Ruggiero, 2016). As such, *col14a1a* and *col14a1b* might have evolved independently and fulfill completely different functions in zebrafish.

To study ColXIV-A functions in more details, we have generated a zebrafish knockout line using CRISPR/Cas9 technology. This new line developed normally and reach adulthood without any delay or visible damage. However, we cannot exclude that embryos harbor subtle phenotypes during embryogenesis as previously shown with knockdown experiments [12]; but if so, it did not drastically impact long term development. We showed that ColXIV-A invalidation did not affect the speed of regeneration nor the overall structure of the outgrowth. However, a detailed analysis of the BM in *col14a1a*$^{-/-}$ pointed to a local and transient role of ColXIV-A in the regenerative BM. First, lack of ColXIV-A specifically impacted laminins deposition which accumulated in the basal epidermal cells in 3 dpa *col14a1a*$^{-/-}$ fish while collagen IV or Amaco deposition in the BM was unaltered. This is in agreement with the fact that both *laminin* and *col14a1a* genes follow similar kinetics of expression and peaked at 2-3 dpa while collagen IV genes were expressed later. ColXIV-A and laminins deposition in the ECM might involve common signaling pathways. Independent studies suggested that ColXIV-A expression and deposition respond to distinct signaling pathways. While TGF-β signaling pathway [40] and retinoic acid [41] were shown to regulate respectively expression of *col14a1* in mammalian cell culture and *col14a1a* in developing zebrafish embryos, BMP signaling regulated specifically the deposition of ColXIV-A in the extracellular space during zebrafish caudal fin regeneration [42]. In agreement with these data, our analysis of the signaling pathways differentially regulated during fin regeneration pinpointed that most of them, including BMP, are very dynamically regulated suggesting an active role in *col14a1a* and *laminin* genes expression.

We have shown that ColXIV-A localized to the BM and that its absence altered proper laminins deposition. Laminins and collagen IV networks are essential for proper mechanical properties of BM. We took advantage of recent developments in AFM to show that lack of ColXIV-A deposition in the BM resulted in a disorganized structure that was thinner but stiffer. Remarkably, the impact of collagen XIV on tissue biomechanics was already pinpointed using cells cultivated in 3D collagen gels in decades [43]. More recently, it was reported that *Col14a1*$^{-/-}$ mice exhibit altered biomechanical properties of the skin [13]. Tomography reconstructions revealed a complete different organization of the BM between WT and *col14a1a*$^{-/-}$ regenerating fins at the nanoscale level. The striking checkerboard pattern made of regularly alternated soft and stiff areas we observed in BM of WT was completely disrupted in *col14a1a* mutants. In mutant BM, soft regions were lacking resulting in a more compact structure. AFM also pointed to a transient role of ColXIV-A in the organization of BM as changes in BM thickness and stiffness were not observed in mature caudal fins of mutants at 1-month post amputation. This transient role of ColXIV-A is in accordance with previous study showing that Collagen XIV regulates tendon fibrillogenesis only during early developmental stages [13]. Our results underscored a regulatory function for Collagen XIV in ECM formation during a narrow time window.

Besides BM toolkit, other BM components also play important functions in the structure and integrity of BM. Collagen VII or XVII mutations in humans induce skin blistering after rupture of the dermoepidermal junction [44]. Together, our study and others demonstrated that BM-associated proteins are also crucially involved in BM organization and biomechanics. However, the mechanisms by which ColXIV-A acts on BM biomechanical properties remain elusive as Collagen XIV binding partners are not clearly identified. The collagenous domains of Collagen XIV were shown to interact with the small proteoglycan Decorin to mediate its interaction with tendon collagen fibrils [45,46] and to the Cartilage Oligomeric Matrix Protein (COMP) protein in dermis [47]. No binding partner has been identified for the long N-terminal non-collagenous domain of ColXIV-A, so far. However, Collagen XIV contains a VWA domain at its N-terminal extremity whose function is to mediate protein-protein interactions [48]. ColXIV-A collagenous domains could thus interact with dermal collagen fibrils and the N-terminal parts of ColXIV-A that was shown to form a trident [49,50] could bind directly or indirectly to BM integral components such as laminins, as illustrated in Figure S10. Loss of ColXIV-A could compromise this protein network resulting in changes in BM biomechanics. Overall, our findings

suggest that ColXIV-A functions as a molecular spacer that is transiently but specifically required for proper 3D-dimensional organization of regenerating BM and integration of laminins within the regenerative BM (Figure S10). Interestingly, overexpression of the C-terminal domain of collagen XVIII, endostatin, another BM component located at the outer surface of the epidermal BM zone, resulted in BM widening [51]. We thus proposed that the 3D-organization of BM is fine-tunely regulated by minor components of the BM zone while the integral components of BM are involved in the assembly of its backbone.

4. Materials and Methods

4.1.Zebrafish husbandry

The following zebrafish strains were used in this study: wild-type AB/Tü or *col14a1a* mutants. Fish were maintained at 28°C in the 'Plateau de Recherche Expérimentale en Criblage *In Vivo*' (PRECI) fish facility (UMS 3444, SFR Biosciences Gerland Lyon Sud, agreement number B693870602). Only females between 8 to 18 months were used for regeneration experiments. Fish were anesthetized in 168 µg/ml of Tricaine (Sigma-Aldrich, St Louis, Missouri, USA) and caudal fin amputations were performed using a scalpel before the ray bifurcations of the caudal fin (Figure S1). For regenerate sampling at later stages (2, 3, 4 and 10 dpa), fins were re-amputated at the exact same location that can be macroscopically identified until 10 dpa. All procedures have been approved by the Ministry of Higher Education and Research and the Ministry of Agriculture and Fisheries.

To monitor the speed of regeneration, pictures of the regenerating fins were taken at 0, 1, 2, 3, 4, 5, 7, 10, 15 and 20 dpa. Six fish of each genotype were used. Ten measurements of the fin outgrowth length were performed using the ImageJ software on each fin. Mean size of the outgrowth of six different fish were used for statistics.

4.2. Genome editing using CRISPR/Cas9 system

sgRNA target sequence was determined using CRISPOR (crispor.tefor.net) and CRISPR direct (crispr.dbcls.jp) software based on Ensembl (ensembl.org) sequence of the *col14a1a* sequence (ENSDARG00000005762). The corresponding pair of designed oligonucleotides were annealed and cloned into the BsaI-digested DR274 plasmid (#42250, Addgene, Cambridge Massachussets, USA) using Quick Ligation kit (New England BioLabs Inc., Ipswich, MA, USA). The resulting sgRNA expressing vector was verified by sequencing. For sgRNA synthesis, template DNA was linearized by DraI digestion and purified using Nucleospin Gel and PCR Clean-Up (Macherey-Nagel, Duren, Germany). The MEGAscript T7 Transcription kit (Thermo Fisher Scientific, Waltham, Massachussets, USA) was used for sgRNA *in vitro* transcription. The sgRNA was purified by ammonium acetate precipitation and stored at -80°C until injection.

One-cell stage embryos were injected with a mix of 133 pg of sgRNA and 2.10 ng of recombinant Cas9 protein (New England BioLabs Inc.) in a final volume of 1nL. 25 embryos were used to assess

the mutagenesis rate using High Resolution Melting Analysis as previously described in Talbot and Amacher, 2014 [52].

4.3. Genotyping

For gDNA extraction, embryos or fin clip were placed in PCR tubes in 100µL of NaOH 50mM, incubated 10 min at 95°C and immediately placed on ice. 10µL of Tris-HCl 1M pH8 were added to buffer the solution and gDNA were stored at 4°C. A three primer-PCR was set up for genotyping. PCR primers were designed using Primer 3 Plus software (www.bioinformatics.nl/cgi-bin/primer3plus/primer3plus.cgi). The three primer-PCR contained two forward primers: one specific for the wild type allele (5' - TATTGGGCGAATCAATTTCCGT -3') and the other one for the mutated allele (5' - GGCGAATCAATTTCTGGTCC -3'); and a common reverse primer (5' - GATGAGACTCACCAATCCTGG -3'). It resulted in two amplicons with 10 nucleotides of difference in size. Amplicons were run in a 4% agarose gel (Figure S5b).

4.4. Morpholinos knockdown

Vivo-morpholinos (MO) against *col14a1a* (5'-CGACACCTGCATCCTTACAGCCAAG-3') and mismatch controls (5'-CGAgACgTGCATaCTTAgAGCgAAG-3') (Gene Tools LLC, Philomath, Oregon, USA) were injected at 2 dpa. MOs were injected using borosilicate needles mounted on a micro-injector in the dorsal half of the caudal fin and the ventral un-injected part was used as an internal control.

4.5. RNA extraction and quantitative real time PCR

Total RNA was isolated using a dedicated kit according to manufacturer instructions (NucleoSpin RNA XS, Macherey-Nagel). Reverse transcription was performed using the M-MLV reverse transcriptase (Promega, Fitchburg, Wisconsin, USA) for 1h at 37°C in presence of both oligo dT and random hexamers (Promega). qPCR primers were designed to obtain amplicons about 200 bp with a 60°C annealing temperature. qPCR was performed using a SYBR Green mix and fast amplification protocol according to manufacturer instructions (Roche, Penzberg, Germany). Data were analyzed using the ΔΔCt method and normalized to *rpl13α*.

4.6. Riboprobe synthesis for in situ hybridization

The riboprobes used were the same as previously published by Bader and collaborators [12]. Riboprobe synthesis was performed by PCR generation of template as previously described in Thisse and Thisse [53], using a T7 promoter. *In vitro* transcription was performed 2h at 37°C using 1µg of linearized DNA, 1X transcription buffer (Promega), 17U of T7 polymerase (Promega), 1X NTP-DIG-RNA (Roche) and 40U of RNAse (Promega). DNA was then digested for 30 min at 37°C by adding 2U of RQ1 RNase-Free DNase (Promega) and 10X of DNase reaction buffer (Promega). The reaction was stopped by adding 2µL of RQ1 DNAse stop solution (Promega) for 10 min at 65°C. The probe was recovered using LiCl precipitation.

4.7. Whole mount in situ hybridization

Caudal fins were collected at 2 or 3 dpa and fixed in 4% (w/v) paraformaldehyde (PFA) in PBS overnight at 4°C. The fixative solution was then replaced by 100% methanol and fins were stored at -20°C. *In situ* hybridization was performed as previously described in Thisse and Thisse [53]. For permeabilization, fins were incubated 30 min with proteinase K. The probe was used at $1/100^{e}$ and the anti-DIG antibody at $1/2000^{e}$. Labeled caudal fins were embedded in 1.5% (w/v) agarose / 5% (w/v) sucrose in PBS and the agarose blocks were kept overnight in 30% sucrose in PBS at 4°C. Agarose blocks were then immersed in OCT freezing medium and snap frozen in isopentenyl (Sigma-Aldrich) pre-cooled at -80°C. Subsequently, 16µm thick sections were performed using a cryostat at -22°C (Leica CM3050 S).

4.8. RNA sequencing

RNA sequencing experiments were performed by the IGFL sequencing platform (Lyon, France). RNA sequencing was performed on three replicates for each condition. Each replicate was constituted by a pool of the outgrowths of six different fish in order to buffer individual variability. Sampling was performed for each replicate as follows: at 0 dpa, the caudal fin of 24 different fish were amputated as described in section 4.1. Six samples were pooled for the 0 dpa time point. At 2 dpa, outgrowths of six other fishes were harvested after re-amputation of the fins at the exact site of initial amputation. The same process was performed at 3 and 10 dpa on six different fish each time.

Time-course experiment during zebrafish caudal fin regeneration was performed on a SOLiD Wildfire sequencer (Thermo Fisher Scientific). Caudal fin samples were stored in lysis buffer at -80°C until RNA extraction. RNA extraction was performed with a NucleoSpin RNA XS kit (Macherey-Nagel), according to manufacturer instructions, except that the carrier RNA was not added. RNA quantity and quality were checked using Qubit 2.0 (Thermo Fisher Scientific) and TapeStation 2200 using a RNA Screentape Assay (Agilent Technologies, Santa Clara, California, USA). All samples had RNA Integrity Number (RIN) ≥ 9. Barcoded libraries were built using SENSE mRNA-Seq Library Prep Kit (Lexogen, Vienna, Austria) dedicated for SOLiD sequencers. The SOLiD libraries constructed for the 5500 system were converted to the 5500W system in order to be compatible with the SOLiD Wildfire sequencer (Thermo Fisher Scientific). For SOLiD reads (50bp), the mapping was performed in color space using the dedicated Lifescope pipeline and the whole.transcriptome.frag workflow on the Ensembl zebrafish genome Zv9 (release October 2014) and using the default parameters. Differential expression analysis on the SOLiD data and Gene Ontology group analyses were performed by Altrabio company (Lyon, France). Raw data have been deposited at NCBI's Gene Expression Omnibus and are accessible through GEO series accession number XXXX.

4.9. Protein extraction and western blot analyses

Proteins were extracted using the following lysis buffer: 150mM NaCl, 50mM Hepes pH7.4, 5mM EDTA, 10% (v/v) glycerol and 1% (v/v) NP-40 supplemented with 1X protease inhibitors cocktail (Roche). Protein concentration was determined using a BCA assay (Thermo Fisher Scientific).

For western blot analyses, samples were separated by SDS-PAGE and blotted onto PVDF membranes. Specific antibodies were used: anti-ColXIV-A [12] 1/2500[e], anti-ColXII [54] 1/2500[e] and anti-β-actin (1/2500[e], A1978, Sigma-Aldrich). Anti-rabbit or anti-mouse HRP-coupled secondary antibodies (1/10000[e], Biorad, Hercules, California, USA) were used with a dedicated kit (170-5070, Biorad) to reveal the proteins with a ChemiDoc (Biorad). Quantitative analyses were performed using the ImageLab software (Biorad).

4.10. Immunostaining

Sections were obtained as described for *in situ* hybridization. For Collagen IV staining, fins were fixed in Dent's fixative solution. Sections were rehydrated 5min in PBS and saturated 30min in blocking

solution (3% (v/v) sheep serum, 1% (w/v) BSA in PBS). Sections were incubated 1h with primary antibodies (anti-ColXIV-A or anti-ColXII, 1/250[e]; L9393, anti-Laminin, Sigma 1/200[e]; Ab23730, anti-collagen I, Abcam, Cambridge, United Kingdom; Ab6586, anti-collagen IV, Abcam; anti-Amaco, kindly provided by R. Wagener) in blocking solution and then washed four times in PBS, 5min each. Sections were incubated 1h with secondary antibodies (Alexa fluor 546 or 488 coupled, Invitrogen, 1/500[e]) and washed twice in PBS, 5min each. Nuclei were then stained 5 min with 0,5 µg/mL Hoechst (Sigma-Aldrich) and washed 5min in PBS before mounting in Dako fluorescence mounting medium (Agilent). Observations were performed using a confocal LSM780 microscope (Zeiss, Oberkochen, Germany).

4.11. Transmission Electron Microscopy

Caudal fins were fixed in 1.5% (v/v) glutaraldehyde, 1% (w/v) PFA in 0.1 M cacodylate buffer (pH 7.4) overnight at 4°C. Samples were washed in 0.1M cacodylate buffer, 10% sucrose twice for 1h each. After post-fixation in 1% osmium tetraoxide for 1h at room temperature, samples were dehydrated in graded series of ethanol (from 30% to 100%) and embedded in epoxy resin. Ultra-thin sections of 65 nm thick were performed and stained with uranyl acetate and lead citrate diluted in methanol. Contrasted sections were observed with a Philips CM120 electron microscope equipped with a Gatan Orius 200 2 K×2 K digital numeric camera (Centre Technologique des Microstructures, Université Lyon 1, France).

4.12. Atomic Force Microscopy

AFM experiments were performed by BioMeca (Lyon, France). At 3 dpa, longitudinal sections of caudal fins were used instead of transversal sections that were preferred at 0 dpa due to the presence of the bony rays that prejudiced AFM measurements. The orientation of fin sections did not impact AFM analysis as shown in Figure 6e and f where similar results were obtained for WT fish at 0 dpa (longitudinal) and 3 dpa (transversal). For all AFM experiments a minimum of three different fish was used. The number of sections that were analyzed is indicated in Table S3. All measurements were performed on a restricted area located in the middle of the outgrowth. As shown in Figure 8a, the epidermal BM appeared as a distinguishable thin and stiff region. In all sections, the width of this region was measured to determine BM thickness. AFM indentation experiments were carried out with

a Catalyst Bioscope (Bruker Nano Surface) mounted on an optical macroscope (MacroFluo, Leica, Wetzlar, Germany) with a 10X objective. A Nanoscope V controller and Nanoscope software versions 8.15 were used. All quantitative measurements were performed using standard pyramidal tips (Scanasyst Air). The tip radius was 20nm according to the manufacturer. The spring constant of cantilevers was measured using the thermal tuning method [55,56] and was ranged from 0.2-0.8 N/m. The deflection sensitivity of cantilevers was calibrated against a clean silicon wafer. All experiments were made in 1X PBS at room temperature and the standard cantilever holder for operation in liquid was used. Samples were positioned on an XY motorized stage and held by a magnetic clamp. The AFM head was then mounted on the stage and an approximated positioning with respect to the cantilever was done using the optical macroscope.

To record surface topology and to create an elastic modulus map, PeakForce QNM AFM mode was used. The foundation of material property mapping with PeakForce QNM is the ability of the system to acquire and analyze the individual force curves from each tap that occurs during the imaging process. To record force, curve the contact mode was used. The foundation of material property mapping with contact mode is the ability of the system to acquire and analyze the individual force curves from each tap that occurs during the acquisition. Each AFM measurements consisted in the analysis of 100 force curves extracted from 10 x 10 matrices with indentation points spaced 15 nm apart. The Young's moduli segments were used to build the 3D matrix that constituted the stiffness tomography data set [30].

In both techniques, the elastic modulus was derived from the FD curves by using the Hertz–Sneddon model [57]. It assumed a rigid cone indenting a flat surface: $F=(2/\pi).(Es/(1-v2s)).\tan(\alpha).\delta 2$ where F is the force from force curve; Es is the Young's modulus; v is the Poisson's ratio; α is the half-angle of the indenter and δ is the indentation. We assumed that samples were perfectly incompressible so that the Poisson's ratio used is 0.5. Since neither the Poisson's ratio nor the tip shape was accurately known, we reported in this work only an 'apparent modulus' (Ea).

4.13. Statistical analyses

Results are given as the means ± SEM. Data significance was analyzed using the Graph Pad Prism 7 (La Jolla, California, USA) version software.

Acknowledgments

We acknowledge the contribution of SFR Biosciences (UMS3444/CNRS, US8/Inserm, ENS de Lyon, UCBL) facilities: PRECI, especially Laure Bernard and Robert Renard, for their help. We are very grateful to Raimund Wagener for kindly providing us the anti-Amaco antibody and to Manuel Koch for helpful discussion on the project. PN is a recipient of a 2016 French Fellowship L'Oréal-UNESCO For Women in Science, the French government (NMRT) and the "Fondation pour la Recherche Médicale" (FDT20160435169) fellowships. This work was supported by the "Agence Nationale pour la Recherche" (ANR) (ANR-16-CE18-0023-03) to FR and the CNRS (CoopIntEer grant).

References

[1] M. Gemberling, T.J. Bailey, D.R. Hyde, K.D. Poss, The zebrafish as a model for complex tissue regeneration., Trends Genet. 29 (2013) 611–20. doi:10.1016/j.tig.2013.07.003.

[2] C. Pfefferli, A. Jaźwińska, The art of fin regeneration in zebrafish, Regeneration. 2 (2015) 72–83. doi:10.1002/reg2.33.

[3] K.D. Poss, M.T. Keating, A. Nechiporuk, Tales of regeneration in zebrafish., Dev. Dyn. 226 (2003) 202–10. doi:10.1002/dvdy.10220.

[4] A.L. Fidler, C.E. Darris, S. V. Chetyrkin, V.K. Pedchenko, S.P. Boudko, K.L. Brown, W. Gray Jerome, J.K. Hudson, A. Rokas, B.G. Hudson, Collagen iv and basement membrane at the evolutionary dawn of metazoan tissues, Elife. 6 (2017) 1–24. doi:10.7554/eLife.24176.001.

[5] C. Frantz, K.M. Stewart, V.M. Weaver, The extracellular matrix at a glance., J. Cell Sci. 123 (2010) 4195–4200. doi:10.1242/jcs.023820.

[6] R.O. Hynes, The extracellular matrix: not just pretty fibrils., Science. 326 (2009) 1216–9. doi:10.1126/science.1176009.

[7] R.O. Hynes, The evolution of metazoan extracellular matrix., J. Cell Biol. 196 (2012) 671–9. doi:10.1083/jcb.201109041.

[8] C. Has, A. Nyström, Epidermal Basement Membrane in Health and Disease, Curr. Top. Membr. 76 (2015) 117–170. doi:10.1016/bs.ctm.2015.05.003.

[9] M. Takeo, W. Lee, M. Ito, Wound healing and skin regeneration, Cold Spring Harb. Perspect. Med. 5 (2015) 1–12. doi:10.1101/cshperspect.a023267.

[10] M. Randles, M.J. Humphries, R. Lennon, Proteomic definitions of basement membrane composition in health and disease, Matrix Biol. (2016). doi:10.1016/j.matbio.2016.08.006.

[11] P. Nauroy, S. Hughes, A. Naba, F. Ruggiero, The in-silico zebrafish matrisome: A new tool to study extracellular matrix gene and protein functions, Matrix Biol. (2017) 1–9. doi:10.1016/j.matbio.2017.07.001.

[12] H.L. Bader, E. Lambert, A. Guiraud, M. Malbouyres, W. Driever, M. Koch, F. Ruggiero, Zebrafish collagen XIV is transiently expressed in epithelia and is required for proper function of certain basement membranes., J. Biol. Chem. (2013). doi:10.1074/jbc.M112.430637.

[13] H.L. Ansorge, X. Meng, G. Zhang, G. Veit, M. Sun, J.F. Klement, D.P. Beason, L.J. Soslowsky, M. Koch, D.E. Birk, Type XIV Collagen Regulates Fibrillogenesis: PREMATURE COLLAGEN FIBRIL GROWTH AND TISSUE DYSFUNCTION IN NULL MICE., J. Biol. Chem. 284 (2009) 8427–38. doi:10.1074/jbc.M805582200.

[14] C. Hemmavanh, M. Koch, D.E. Birk, E.M. Espana, Abnormal corneal endothelial maturation in collagen XII and XIV null mice., Invest. Ophthalmol. Vis. Sci. 54 (2013) 3297–308. doi:10.1167/iovs.12-11456.

[15] G. Tao, A.K. Levay, J.D. Peacock, D.J. Huk, S.N. Both, N.H. Purcell, J.R. Pinto, M.L. Galantowicz, M. Koch, P.A. Lucchesi, D.E. Birk, J. Lincoln, Collagen XIV is important for growth and structural integrity of the myocardium., J. Mol. Cell. Cardiol. 53 (2012) 626–38. doi:10.1016/j.yjmcc.2012.08.002.

[16] L.T. Tomte, A.S. Geiser, A. Hansen, F. Tesche, R. Herken, N. Miosge, Collagen types XII and XIV are present in basement membrane zones during human embryonic development., J. Mol. Histol. 35 (2004) 803–10. doi:10.1007/s10735-004-1132-y.

[17] D. Wehner, G. Weidinger, Signaling networks organizing regenerative growth of the zebrafish fin, Trends Genet. 31 (2015) 336–343. doi:10.1016/j.tig.2015.03.012.

[18] T.J. Carney, N.M. Feitosa, C. Sonntag, K. Slanchev, J. Kluger, D. Kiyozumi, J.M. Gebauer, J.C. Talbot, C.B. Kimmel, K. Sekiguchi, R. Wagener, H. Schwarz, P.W. Ingham, M. Hammerschmidt, Genetic analysis of fin development in zebrafish identifies furin and Hemicentin1 as potential novel fraser syndrome disease genes, PLoS Genet. 6 (2010). doi:10.1371/journal.pgen.1000907.

[19] C.-H. Chen, A.F. Merriman, J. Savage, J. Willer, T. Wahlig, N. Katsanis, V.P. Yin, K.D. Poss, Transient laminin beta 1a Induction Defines the Wound Epidermis during Zebrafish Fin Regeneration., PLoS Genet. 11 (2015) e1005437. doi:10.1371/journal.pgen.1005437.

[20] K. Short, F. Wiradjaja, I. Smyth, Let's stick together: the role of the Fras1 and Frem proteins in epidermal adhesion., IUBMB Life. 59 (2007) 427–35. doi:10.1080/15216540701510581.

[21] S.H. Kim, H.Y. Choi, J.-H. So, C.-H. Kim, S.-Y. Ho, M. Frank, Q. Li, J. Uitto, Zebrafish type XVII collagen: gene structures, expression profiles, and morpholino "knock-down" phenotypes., Matrix Biol. 29 (2010) 629–37. doi:10.1016/j.matbio.2010.07.002.

[22] L. Nahidiazar, M. Kreft, B. van den Broek, P. Secades, E.M.M. Manders, a. Sonnenberg, K. Jalink, The molecular architecture of hemidesmosomes as revealed by super-resolution microscopy, J. Cell Sci. 128 (2015) 3714–9. doi:10.1242/jcs.171892.

[23] M. Nishimura, W. Nishie, Y. Shirafuji, S. Shinkuma, K. Natsuga, H. Nakamura, D. Sawamura, K. Iwatsuki, H. Shimizu, Extracellular cleavage of collagen XVII is essential for correct cutaneous basement membrane formation, Hum. Mol. Genet. 25 (2016) 328–339. doi:10.1093/hmg/ddv478.

[24] R.J. Richardson, J.M. Gebauer, J. Zhang, B. Kobbe, D.R. Keene, K.R. Karlsen, S. Richetti, A.P. Wohl, G. Sengle, W.F. Neiss, M. Paulsson, M. Hammerschmidt, R. Wagener, AMACO is a component of the basement membrane-associated Fraser complex., J. Invest. Dermatol. 134 (2014) 1313–22. doi:10.1038/jid.2013.492.

[25] S. Hiroyasu, J.C.R. Jones, A new component of the Fraser complex., J. Invest. Dermatol. 134 (2014) 1192–3. doi:10.1038/jid.2013.514.

[26] S.E. Mercer, S.J. Odelberg, H.G. Simon, A dynamic spatiotemporal extracellular matrix facilitates epicardial-mediated vertebrate heart regeneration, Dev. Biol. 382 (2013) 457–469. doi:10.1016/j.ydbio.2013.08.002.

[27] A. Pozzi, P.D. Yurchenco, R. V. Iozzo, The nature and biology of basement membranes, Matrix Biol. (2016). doi:10.1016/j.matbio.2016.12.009.

[28] F.L. Chan, S. Inoue, Lamina lucida of basement membrane: An artefact, Microsc. Res. Tech. 28 (1994) 48–59. doi:10.1002/jemt.1070280106.

[29] F. Chablais, A. Jazwinska, IGF signaling between blastema and wound epidermis is required

for fin regeneration., Development. 137 (2010) 871–9. doi:10.1242/dev.043885.

[30] C. Roduit, S. Sekatski, G. Dietler, S. Catsicas, F. Lafont, S. Kasas, Stiffness tomography by atomic force microscopy, Biophys. J. 97 (2009) 674–677. doi:10.1016/j.bpj.2009.05.010.

[31] S. Ricard-Blum, F. Ruggiero, The collagen superfamily: from the extracellular matrix to the cell membrane., Pathol. Biol. (Paris). 53 (2005) 430–42. doi:10.1016/j.patbio.2004.12.024.

[32] J. Govindan, M.K. Iovine, Dynamic remodeling of the extra cellular matrix during zebrafish fin regeneration., Gene Expr. Patterns. 19 (2015) 21–9. doi:10.1016/j.gep.2015.06.001.

[33] I. Duran, F. Csukasi, S.P. Taylor, D. Krakow, J. Becerra, a Bombarely, M. Marí-Beffa, Collagen duplicate genes of bone and cartilage participate during regeneration of zebrafish fin skeleton., Gene Expr. Patterns. 19 (2015) 60–9. doi:10.1016/j.gep.2015.07.004.

[34] P.D. Yurchenco, B.L. Patton, Developmental and pathogenic mechanisms of basement membrane assembly., Curr. Pharm. Des. 15 (2009) 1277–94. doi:10.2174/138161209787846766.

[35] E. Pavlakis, R. Chiotaki, G. Chalepakis, The role of Fras1/Frem proteins in the structure and function of basement membrane, Int. J. Biochem. Cell Biol. 43 (2011) 487–495. doi:10.1016/j.biocel.2010.12.016.

[36] P. Petrou, A.K. Makrygiannis, G. Chalepakis, The fras1/frem family of extracellular matrix proteins: Structure, function, and association with fraser syndrome and the mouse bleb phenotype, Connect. Tissue Res. 49 (2008) 277–282. doi:10.1080/03008200802148025.

[37] A. Pagnon-Minot, M. Malbouyres, Z. Haftek-Terreau, H.R. Kim, T. Sasaki, C. Thisse, B. Thisse, P.W. Ingham, F. Ruggiero, D. Le Guellec, Collagen XV, a novel factor in zebrafish notochord differentiation and muscle development, Dev. Biol. 316 (2008) 21–35. doi:10.1016/j.ydbio.2007.12.033.

[38] S. Bretaud, A. Pagnon-Minot, E. Guillon, F. Ruggiero, D. Le Guellec, Characterization of spatial and temporal expression pattern of Col15a1b during zebrafish development, Gene Expr. Patterns. 11 (2011) 129–134. doi:10.1016/j.gep.2010.10.004.

[39] E. Guillon, S. Bretaud, F. Ruggiero, Slow Muscle Precursors Lay Down a Collagen XV Matrix Fingerprint to Guide Motor Axon Navigation, J. Neurosci. 36 (2016) 2663–2676. doi:10.1523/JNEUROSCI.2847-15.2016.

[40] K. Arai, Y. Kasashima, A. Kobayashi, A. Kuwano, T. Yoshihara, TGF-beta alters collagen XII and XIV mRNA levels in cultured equine tenocytes., Matrix Biol. 21 (2002) 243–50. http://www.ncbi.nlm.nih.gov/pubmed/12009330.

[41] E. Samarut, C. Gaudin, S. Hughes, B. Gillet, S. de Bernard, P.-E. Jouve, L. Buffat, A. Allot, O. Lecompte, L. Berekelya, C. Rochette-Egly, V. Laudet, Retinoic acid receptor subtype-specific transcriptotypes in the early zebrafish embryo., Mol. Endocrinol. 28 (2014) 260–72. doi:10.1210/me.2013-1358.

[42] V. Thorimbert, D. König, J. Marro, F. Ruggiero, A. Jaźwińska, Bone morphogenetic protein signaling promotes morphogenesis of blood vessels, wound epidermis, and actinotrichia during fin regeneration in zebrafish, FASEB J. 29 (2015) 4299–4312. doi:10.1096/fj.15-272955.

[43] T. Nishiyama, a M. McDonough, R.R. Bruns, R.E. Burgeson, Type XII and XIV collagens mediate interactions between banded collagen fibers in vitro and may modulate extracellular matrix deformability., J. Biol. Chem. 269 (1994) 28193–9. http://www.ncbi.nlm.nih.gov/pubmed/7961756.

[44] C. Has, L. Bruckner-Tuderman, The genetics of skin fragility., Annu. Rev. Genomics Hum. Genet. 15 (2014) 245–68. doi:10.1146/annurev-genom-090413-025540.

[45] B. Font, E. Aubertfoucher, D. Goldschmidt, D. Eichenberger, M. VanderRest, Binding of Collagen-XIV with the Dermatan Sulfate Side-Chain of Decorin, J. Biol. Chem. 268 (1993) 25015–25018. isi:A1993MG67300074.

[46] T. Ehnis, W. Dieterich, M. Bauer, H. Kresse, D. Schuppan, Localization of a binding site for the proteoglycan decorin on collagen XIV (undulin)., J. Biol. Chem. 272 (1997) 20414–9. http://www.ncbi.nlm.nih.gov/pubmed/9252349.

[47] P. Agarwal, D. Zwolanek, D.R. Keene, J.-N. Schulz, K. Blumbach, D. Heinegård, F. Zaucke, M. Paulsson, T. Krieg, M. Koch, B. Eckes, Collagen XII and XIV, new partners of cartilage oligomeric matrix protein in the skin extracellular matrix suprastructure., J. Biol. Chem. 287 (2012) 22549–59. doi:10.1074/jbc.M111.335935.

[48] C.A. Whittaker, R.O. Hynes, Distribution and evolution of von Willebrand/integrin A domains: widely dispersed domains with roles in cell adhesion and elsewhere., Mol. Biol. Cell. 13 (2002) 3369–87. doi:10.1091/mbc.E02-05-0259.

[49] E. Aubert-Foucher, B. Font, D. Eichenberger, D. Goldschmidt, C. Lethias, M. van der Rest, Purification and characterization of native type XIV collagen., J. Biol. Chem. 267 (1992) 15759–64. http://www.ncbi.nlm.nih.gov/pubmed/1322405 (accessed October 21, 2014).

[50] M.K. Gordon, R. a Hahn, Collagens., Cell Tissue Res. 339 (2010) 247–57. doi:10.1007/s00441-009-0844-4.

[51] H. Elamaa, R. Sormunen, M. Rehn, R. Soininen, T. Pihlajaniemi, Endostatin overexpression specifically in the lens and skin leads to cataract and ultrastructural alterations in basement membranes., Am. J. Pathol. 166 (2005) 221–9. doi:10.1016/S0002-9440(10)62246-8.

[52] J.C. Talbot, S.L. Amacher, A streamlined CRISPR pipeline to reliably generate zebrafish frameshifting alleles., Zebrafish. 11 (2014) 583–5. doi:10.1089/zeb.2014.1047.

[53] C. Thisse, B. Thisse, High-resolution in situ hybridization to whole-mount zebrafish embryos., Nat. Protoc. 3 (2008) 59–69. doi:10.1038/nprot.2007.514.

[54] H.L. Bader, D.R. Keene, B. Charvet, G. Veit, W. Driever, M. Koch, F. Ruggiero, Zebrafish collagen XII is present in embryonic connective tissue sheaths (fascia) and basement membranes., Matrix Biol. 28 (2009) 32–43. doi:10.1016/j.matbio.2008.09.580.

[55] J. Hutter, J. Bechhoefer, Calibration of atomic force microscope tips, Rev. Sci. Instrum. 64 (1993) 1868. doi:10.1063/1.1143970.

[56] R. Lévy, M. Maaloum, Measuring the spring constant of atomic force microscope cantilevers: thermal fluctuations and other methods, Nanotechnology. 13 (2002) 33–37.

[57] I.N. Sneddon, The relation between load and penetration in the axisymmetric boussinesq

problem for a punch of arbitrary profile, Int. J. Eng. Sci. 3 (1965) 47–57. doi:10.1016/0020-7225(65)90019-4.